AJNR

Exploratory Multisite Magnetic Resonance Spectroscopic Imaging Shows White Matter Neuroaxonal Loss Associated with Complications of Type 1 Diabetes in Children

L.Y. Cai, C. Tanase, A.W. Anderson, N.J. Patel, C.A. Lee, R.S. Jones, L.M. LeStourgeon, A. Mahon, I. Taki, J. Juvera, S. Pruthi, K. Gwal, A. Ozturk, H. Kang, A. Rewers, M.J. Rewers, G.T. Alonso, N. Glaser, S. Ghetti, S.S. Jaser, B.A. Landman and L.C. Jordan

AJNR Am J Neuroradiol published online 1 June 2023
http://www.ajnr.org/content/early/2023/06/01/ajnr.A7895

Published June 1, 2023 as 10.3174/ajnr.A7895

Exploratory Multisite Magnetic Resonance Spectroscopic Imaging Shows White Matter Neuroaxonal Loss Associated with Complications of Type 1 Diabetes in Children

L.Y. Cai, C. Tanase, A.W. Anderson, N.J. Patel, C.A. Lee, R.S. Jones, L.M. LeStourgeon, A. Mahon, I. Taki, J. Juvera, S. Pruthi, K. Gwal, A. Ozturk, H. Kang, A. Rewers, M.J. Rewers, G.T. Alonso, N. Glaser, S. Ghetti, S.S. Jaser, B.A. Landman, and L.C. Jordan

ABSTRACT

BACKGROUND AND PURPOSE: Type 1 diabetes affects over 200,000 children in the United States and is associated with an increased risk of cognitive dysfunction. Prior single-site, single-voxel MRS case reports and studies have identified associations between reduced NAA/Cr, a marker of neuroaxonal loss, and type 1 diabetes. However, NAA/Cr differences among children with various disease complications or across different brain tissues remain unclear. To better understand this phenomenon and the role of MRS in characterizing it, we conducted a multisite pilot study.

MATERIALS AND METHODS: In 25 children, 6–14 years of age, with type 1 diabetes across 3 sites, we acquired T1WI and axial 2D MRSI along with phantom studies to calibrate scanner effects. We quantified tissue-weighted NAA/Cr in WM and deep GM and modeled them against study covariates.

RESULTS: We found that MRSI differentiated WM and deep GM by NAA/Cr on the individual level. On the population level, we found significant negative associations of WM NAA/Cr with chronic hyperglycemia quantified by hemoglobin A1c ($P < .005$) and a history of diabetic ketoacidosis at disease onset ($P < .05$). We found a statistical interaction ($P < .05$) between A1c and ketoacidosis, suggesting that neuroaxonal loss from ketoacidosis may outweigh that from poor glucose control. These associations were not present in deep GM.

CONCLUSIONS: Our pilot study suggests that MRSI differentiates GM and WM by NAA/Cr in this population, disease complications may lead to neuroaxonal loss in WM in children, and deeper investigation is warranted to further untangle how diabetic ketoacidosis and chronic hyperglycemia affect brain health and cognition in type 1 diabetes.

ABBREVIATIONS: DKA = diabetic ketoacidosis; HbA1c = hemoglobin A1c; MRSI = magnetic resonance spectroscopic imaging; T1D = type 1 diabetes

Type 1 diabetes (T1D) affects almost 1.7 million individuals, including >200,000 children and adolescents in the United States.[1] With time, children with T1D may experience declines in cognitive functions such as memory, attention, and problem solving.[2] These deficits, in turn, may impair subsequent T1D management, leading to further worsening of glycemic control and additional T1D complications.[2] Thus, the public health implications of understanding and preventing cognitive decline in this population are considerable.[3]

Prior neuroimaging studies have uncovered structural brain changes in T1D populations. Poor glycemic control has been negatively correlated with GM and WM growth in children with T1D.[4,5] Furthermore, hippocampal changes have been found in children with dysglycemia, some of which were hypothesized to reflect a response to injury, such as disruption of normal pruning.[6,7] T1D and hyperglycemia have also been negatively associated with localized DTI microstructural measures of brain health.[8]

Received February 18, 2023; accepted after revision May 3.

From the Department of Biomedical Engineering (L.Y.C., A.W.A., B.A.L.), Vanderbilt University Institute of Imaging Science (A.W.A., B.A.L.), and Department of Electrical and Computer Engineering (B.A.L.), Vanderbilt University, Nashville, Tennessee; Departments of Psychiatry and Behavioral Sciences (C.T.) and Psychology (A.M., S.G.), University of California, Davis, Davis, California; Departments of Radiology and Radiological Sciences (A.W.A., S.P., B.A.L.), Pediatrics (N.J.P., R.S.J., S.S.J., L.C.J.), Neurology (C.A.L., L.C.J.), Medicine (L.M.L.), and Biostatistics (H.K.), Vanderbilt University Medical Center, Nashville, Tennessee; Department of Pediatrics (I.T., A.R., M.J.R.), Barbara Davis Center (G.T.A.), and Department of Psychiatry (J.J.), University of Colorado Anschutz Medical Campus, Aurora, Colorado; and Departments of Radiology (K.G., A.O.) and Pediatrics (N.G.), University of California Davis Health, University of California Davis School of Medicine, Sacramento, California.

This work was conducted, in part, by using the resources of the Advanced Computing Center for Research and Education at Vanderbilt University, Nashville, Tennessee and was supported by the National Institutes of Health (under award numbers 1U34DK123895-01, U34DK123894-01, and T32GM007347) and by the National Science Foundation under award number 2040462.

The content is solely the responsibility of the authors and does not necessarily represent the official views of the National Institutes of Health or the National Science Foundation.

Please address correspondence to Leon Y. Cai, Medical-Image Analysis and Statistical Interpretation Lab, 400 24th Ave S, FGH 369, Vanderbilt University, Nashville, TN 37212; e-mail: leon.y.cai@vanderbilt.edu; @LeonCai

Indicates open access to non-subscribers at www.ajnr.org

Indicates article with online supplemental data.

http://dx.doi.org/10.3174/ajnr.A7895

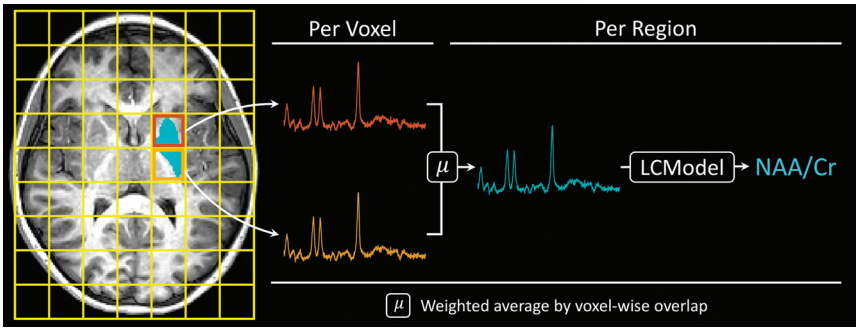

FIG 1. Illustrated MRSI workflow. After acquiring 2D MRSI and an associated TIWI-based segmentation, one spectrum for each region was generated by combining the spectra for all overlapping voxels in a weighted average based on overlap contribution (Equation). The regionally-weighted spectra were subsequently fit using LCModel to compute metabolite peaks, resulting in one metabolite ratio computed per participant per region. Of note, the pictured MRSI grid is provided only for illustrative purposes and does not represent collected data.

Prior studies have also identified similar regional changes in brain function. Differences in activation across the cingulum, hypothalamus, cortex, deep GM nuclei, and other regions have been observed with regard to changes in working memory and visual and motor processes as well as T1D severity.[9-12] Taken together, these studies suggest that not meeting glycemic targets in T1D may be associated with regional changes in brain structure and function but do not directly assess neuronal health or neurochemistry. Thus, the mechanism underlying these changes remains unclear.

Changes to neurochemistry can be measured using MRS. Specifically, the ratio of NAA to Cr (NAA/Cr) is thought to reflect neuronal density and health, with decreasing NAA/Cr values reflecting a decline in normal metabolic functioning and neuronal loss. Prior MRS studies suggest that T1D and/or episodes of diabetic ketoacidosis (DKA) may contribute to reduced NAA/Cr.[13-15] Additionally, associations between reduced NAA/Cr in the frontal regions and reduced cognitive performance have been detected in typically developing children.[16] However, these studies have largely been limited to case reports or single-site, single-voxel studies, and studies have yet to investigate differences across children with various T1D complications or be integrated with regions or tissues defined on structural MR imaging to explore differences localized to different parts of the brain.[13-15,17]

Thus, to further understand the effects of T1D on the brain and the role of MRS and MR imaging in characterizing them across different tissue regions, we conducted a multisite pilot study using tissue-weighted 2D magnetic resonance spectroscopic imaging (MRSI) in hopes of motivating larger neuroimaging studies of this population. We hypothesized that children with T1D and increased exposure to hyperglycemia, indicated by higher hemoglobin A1c (HbA1c), would exhibit lower NAA/Cr compared with children with T1D with less exposure to hyperglycemia. Furthermore, we hypothesized that a history of DKA may contribute to these differences and explored whether this finding may be localized to certain tissues or regions across the brain.

MATERIALS AND METHODS

Study Cohort and Imaging Acquisitions

We imaged 25 children 6–14 years of age with T1D with no contraindications to MR imaging or other major medical conditions across 3 sites: A, B, and C. We acquired 3D T1WI and 2D chemical shift MRSI. At site A, all images were acquired on a 3T Achieva scanner (Philips Healthcare); at site B, on a 3T Tim Trio scanner (Siemens); and at site C, on a 3T Magnetom Skyra scanner (Siemens). We also recorded each participant's sex, age at imaging, duration of T1D (defined as time between diagnosis and imaging), whether they presented in DKA at diagnosis, HbA1c assessed once within 3 months of imaging, and race. All HbA1c measurements were obtained with point-of-care tests conducted at regular diabetes clinic visits except for 1 participant at site A whose HbA1c value was obtained with venipuncture.

T1WI was acquired at 1.0-mm isotropic resolution with TE/TR = 2.9/6310 ms at site A and 3.5/2500 ms at sites B and C. MRSI was acquired with 2D point-resolved spectroscopy sequences in an axial slice at the level of the basal ganglia with suppression bands placed around the skull. Images at site A were acquired with 20 × 24 voxels with TE/TR = 144/2000 ms at 9.58 × 9.58 × 15 mm resolution. Images at sites B and C were acquired with 16 × 16 voxels with TE/TR = 135/1690 ms at 12.5 × 12.5 × 10 mm resolution. The full MRSI parameters are available in the Online Supplemental Data.

Written informed consent and assent was provided by guardians and participants, respectively. This study was approved by the Institutional Review Boards at all sites.

Computing Regionally Weighted Metabolite Ratios

Overall, we used the following: 1) regional segmentations of different tissues derived from T1WI, 2) removed voxels with lipid interference, 3) computed regionally weighted spectra for each participant, and 4) computed metabolite ratios per participant per region.

First, T1WI was segmented using the spatially localized atlas network tiles framework followed by a manual review for quality to obtain a segmentation of the brain, the WM, and 6 deep GM nuclei: right and left caudate, basal ganglia (globus pallidus and putamen), and thalami (Online Supplemental Data).[18]

Second, we excluded MRSI voxels in the brain with large signal interference from lipids. For each participant, we computed the real spectrum for each MRSI voxel within the brain and fit it between 1.8 and 0.2 ppm with a line of best fit. We then computed the root mean square error between the spectrum and the line for each voxel and identified and excluded outliers as those voxels with errors 1.5 times the interquartile range above the 75th or below the 25th percentile.[19]

Third, using the T1WI segmentations and 2D MRSI slabs, we computed regionally weighted spectra for each participant using a weighted average approach (Fig 1). Any given region defined on T1WI overlapped a number of MRSI voxels, indicating that the spectrum for that region was a combination of signals from the overlapping MRSI voxels. Thus, for a region, *r*, we computed

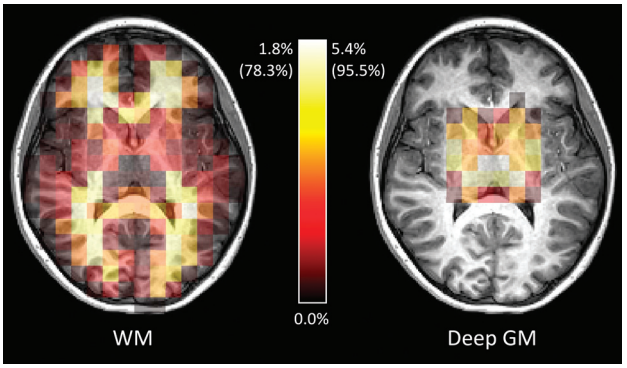

FIG 2. Maps of weights used to compute weighted average spectra for WM and deep GM in a representative participant. Each voxel is colored to represent its percent contribution to the tissue-weighted spectra as well as the corresponding voxel-wise volume fraction in parentheses.

the spectrum of that region, s_r, by taking a weighted average of the signals from the overlapping MRSI voxels, s^i, as shown in the Equation, where v_r is the total volume of region r overlapping the MRSI slab and v_r^i is the volume of region r overlapping the ith MRSI voxel.

$$s_r = \sum_i \frac{v_r^i}{v_r} s^i.$$

We focused on WM and deep GM regions and visualized the percentage contribution of each MRSI voxel to the resultant spectrum of these tissues as well as the analogous tissue volume fractions in a representative participant (Fig 2). The tissue volume fraction for MRSI voxel i was computed as v_r^i/v^i, where v^i is the volume of MRSI voxel i itself. Cortical GM was not analyzed to avoid artifacts from suppression bands placed around the skull.

Fourth, the weighted average spectra for each region for each participant in the time domain were passed into LCModel (http://s-provencher.com/lcmodel.shtml) basis-fitting software to compute metabolite ratios (Fig 1 and Online Supplemental Data).[20] TE-specific 3T basis sets provided by LCModel were used to compute the NAA/Cr from the spectra for each region. Notably, the NAA peaks used for ratio computation were themselves computed from the sum of the NAA and *N*-acetyl aspartylglutamate peaks fit with LCModel. Similarly, the Cr peaks were computed from the sum of the Cr and phosphocreatine peaks. This decision was made in line with recommendations from LCModel because it is difficult to separate NAA from *N*-acetyl aspartylglutamate and Cr from phosphocreatine at 3T. Furthermore, the ratios were filtered on the basis of the %SD metric of the constituent peaks computed by LCModel before analysis. Briefly, %SD is a contrast-to-noise metric representing the Cramér-Rao lower bounds of estimated SDs of the peak fits. All peaks with a %SD of >20% and any associated ratios were removed from consideration, in line with recommendations from LCModel that the %SD threshold be no greater than 20%.

Calibrating Metabolite Ratios among Sites

As detailed in the Online Supplemental Data, we calibrated site-wise differences in TE/TR and observed scanner differences to compare NAA/Cr across sites, in line with prior work noting the need for multisite MRS harmonization, especially with scanners from multiple vendors (Online Supplemental Data).[21-23] Briefly, a Braino MRS phantom (GE Healthcare) was scanned at each site using the same site-specific protocols. We identified the NAA and Cr peaks in the center voxels of the phantom within the VOI with LCModel. We computed the ratio of the median NAA to median Cr values to obtain a site-specific correction factor. For each site, the NAA/Cr ratios computed from participant imaging were subsequently divided by the site's correction factor to normalize among sites.

Associations of NAA/Cr with Complications of T1D

To investigate tissue-weighted associations of NAA/Cr with T1D complications on the population level, we regressed the calibrated ratios in the WM and deep GM against study demographics in a forward model selection process, evaluating the Akaike Information Criterion, adjusted coefficients of determination (R^2), effect sizes, and P values. Specifically, we investigated the relationship of chronic hyperglycemia, DKA, and their interaction with NAA/Cr and subsequently added additional covariates to identify the presence of other effects. Race was omitted due to sample-size limitations. All models included an intercept term that is not presented.

RESULTS

Study Cohort and Regionally Weighted Spectra

The demographics of our study cohort stratified by site are reported in Table 1. The sites were reasonably balanced overall, given this small pilot study, but some differences existed by site, particularly the duration of T1D and DKA at onset. To account for these differences, we calibrated site-wise differences and used statistical models that included these covariates.

The resultant spectra for the WM and deep GM as well as the deep GM split into 6 nuclei are shown via means and 95% confidence intervals across participants (Fig 3). All deep GM spectra have little-to-no lipid interference after voxel exclusion, though the WM spectra have some. This finding is logical because WM extends closer to pericranial fat than deep GM structures do. However, this interference in WM does not qualitatively impact the NAA peaks (2.0 ppm). We also observed that the NAA and Cr (3.0 ppm) peaks demonstrate consistent morphology across participants. We counted the median number of excluded voxels per MRSI image to be 5, indicating roughly <5% excluded voxels per participant. Last, the median number of voxels used in WM ranged from 120 to 130, and in deep GM as a whole, it ranged from 30 to 40. Overall, these spectra were found acceptable for further NAA/Cr analysis.

Tissue-Weighted Differences in Metabolite Ratios

To investigate NAA/Cr differences by tissue, we plotted the ratios across participants in the WM, 6 deep GM nuclei, and deep GM as a whole (Fig 4*A*). We investigated regional differences with pair-wise Wilcoxon signed-rank tests after false discovery rate multiple comparison correction and without calibration because the comparisons were matched within participants and not pooled across sites.

NAA/Cr in the WM was significantly higher than in deep GM generally ($P < .005$) and in the caudate and basal ganglia specifically ($P < .005$ bilaterally) (Fig 4*B*). We also found differences between the WM and right thalamus ($P < .05$) (Fig 4*B*). This difference was not recapitulated on the left, but significant differences were not found between the left and right thalamus (Fig 4*C*). Additionally, left-right symmetric differences were present in deep GM nuclei, with increasing NAA/Cr from the caudate to the basal ganglia ($P < .05$ on the right and $P = .082$ on the left) to the thalamus ($P < .005$ bilaterally) (Fig 4*D*). These results suggest that our methodology identified tissue-weighted differences in NAA/Cr matched within each participant on the individual level and that these differences are largely left-right symmetric.

Associations of NAA/Cr with Complications of T1D

The forward model selection results are reported in Table 2. In the WM, we identified a statistically significant negative association between HbA1c and NAA/Cr, suggesting that elevated HbA1c is associated with decreased NAA/Cr. We also found large changes in the HbA1c and DKA effects with the addition of an interaction term between HbA1c and DKA status: Both effect sizes increased dramatically, the DKA effect became significant, and the interaction term nearly cancelled out the HbA1c effect. Additionally, these glycemic effects alone resulted in the model with the lowest Akaike Information Criterion and highest adjusted R^2. The addition of the age, sex, and duration covariates did not improve the Akaike Information Criterion or noticeably change identified effects, suggesting that these additional covariates did not capture meaningful variance otherwise. In deep GM, no analogous associations in NAA/Cr or drops in the Akaike Information Criterion were identified as more terms were added. Similar findings were observed in a secondary sensitivity analysis with an expanded model selection process incorporating all combinations of variables.

We visualized the WM model with the lowest Akaike Information Criterion in Fig 5. The negative HbA1c effect identified is visually present when considering all sites both together and separately. We also observed the DKA and interaction effects, recognizing small sample sizes and potential confounding by site. For instance, the participants from site C had higher NAA/Cr values, but none had DKA at onset, whereas the participants from site B had lower NAA/Cr values but most had DKA at onset. At site A, where 50% of participants had DKA at onset, no qualitatively appreciable difference in NAA/Cr with DKA was found. These qualitative findings were supported quantitatively when a fixed site effect was added to the models in a secondary sensitivity analysis. The relationship of the glycemic effects to each other remained but were reduced in magnitude and lost significance, as expected. Additionally, in secondary analyses considering the sites separately, similar trends were observed albeit without statistical significance due to further reduced sample sizes, also as expected.

Taken together, these results suggest that T1D effects in NAA/Cr were measurable across sites but potentially at a magnitude smaller than the site effects. Specifically, NAA/Cr in WM decreased both with increasing HbA1c and with DKA, consistent with neuroaxonal loss.

Table 1: Cohort demographics by site

	Site A	Site B	Site C	Overall
Sample size (No.)	10	11	4	25
Age (yr) (mean)	10.6 (SD, 1.1)	10.5 (SD, 2.7)	8.5 (SD, 1.3)	10.2 (SD, 2.0)
Sex, female (No.)	7 (70%)	5 (45%)	3 (75%)	15 (60%)
Duration (yr) (mean)	2.6 (SD, 2.3)	4.6 (SD, 3.3)	0.3 (SD, 0.1)	3.1 (SD, 3.0)
HbA1c (%) (mean)	9.5 (SD, 3.2)	8.5 (SD, 1.9)	6.2 (SD, 0.9)	8.5 (SD, 2.6)
DKA at onset (No.)	5 (50%)	9 (82%)	0 (0%)	14 (56%)
Race (No)				
White	7 (70%)	8 (73%)	4 (100%)	19 (76%)
Black/African American	2 (20%)	1 (9%)	0 (0%)	3 (12%)
Multiracial (black/white)	0 (0%)	1 (9%)	0 (0%)	1 (4%)
Other	1 (10%)	1 (9%)	0 (0%)	2 (8%)

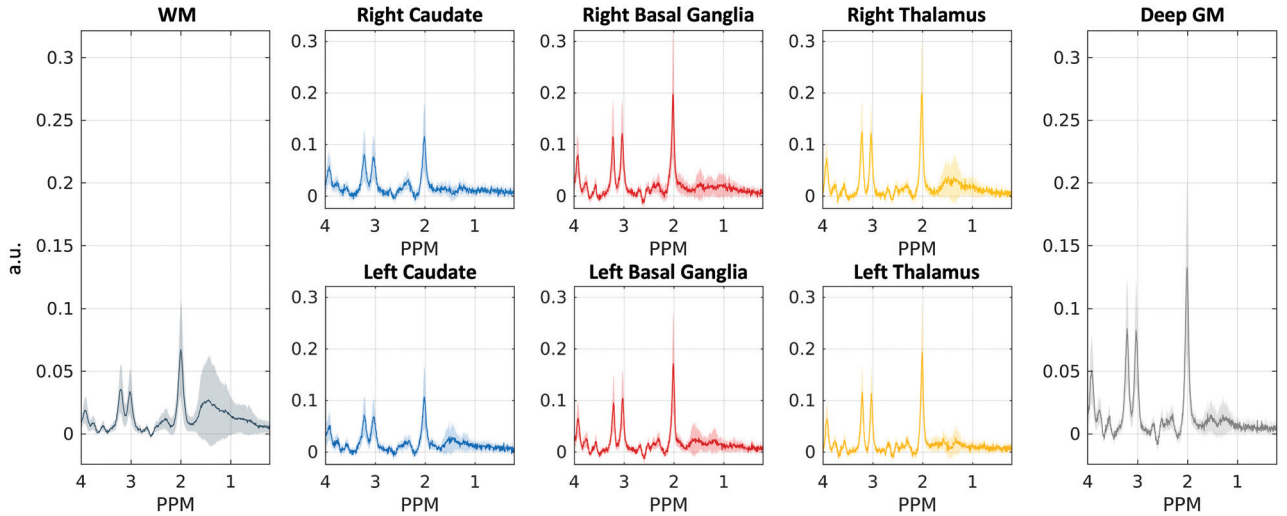

FIG 3. Mean regionally weighted spectra with 95% confidence intervals across participants from 0.2 to 4.0 ppm. Spectra were extracted for each region for each participant from LCModel and plotted after baseline subtraction. a.u. indicates arbitrary units.

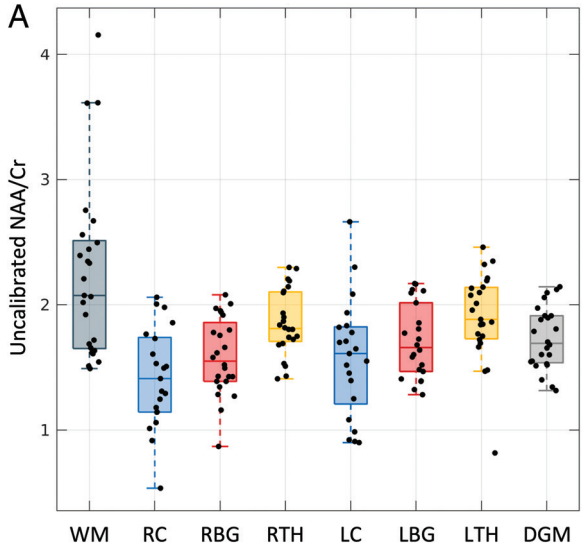

B	WM	RC	RBG	RTH	LC	LBG	LTH	DGM	
WM	–	**	***	*	**	**	ns	**	WM
DGM	**	**	**	*	*	ns	**	–	DGM

C	RC	RBG	RTH		D	RC	RBG	RTH	
LC	*	ns	*	LC	LC		*	**	RC
LBG	**	ns	*	LBG	LBG	0.082		**	RBG
LTH	**	***	ns	LTH	LTH	**	**		RTH
	RC	RBG	RTH			LC	LBG	LTH	

FIG 4. Differences in NAA/Cr in T1D by region. *A*, The uncalibrated NAA/Cr ratios from the regionally weighted spectra are shown across participants. *B*, *P* values of statistical comparisons between WM and deep GM as a whole and the individual deep nuclei. *C*, *P* values of contralateral comparisons in deep GM nuclei. *D*, *P* values of ipsilateral comparisons in deep GM nuclei. Statistical significance between regions was determined with pair-wise Wilcoxon signed-rank tests after false discovery rate correction (en dash indicates not tested; ns, not significant; single asterisk, $P < .05$; double asterisks, $P < .005$; triple asterisks, $P < .0005$). RC indicates right caudate; RBG, right basal ganglia; RTH, right thalamus; LC, left caudate; LBG, left basal ganglia; LTH, left thalamus; DGM, deep GM.

Table 2: Effect sizes, Akaike Information Criterion, and adjusted R^2 for forward model selection of NAA/Cr in WM and deep GM with T1D covariates

Tissue	HbA1c	DKA	HbA1c x DKA	Age	Sex	Duration	Akaike	aR^2
WM	–0.086[a]	–	–	–	–	–	17.581	0.291
	–0.080[b]	–0.095	–	–	–	–	19.083	0.273
	–0.171[a,c]	–1.142[b,c]	0.130[b,c]	–	–	–	15.373[c]	0.394[c]
	–0.169[a]	–1.156[b]	0.131[b]	–0.009	–	–	17.298	0.365
	–0.187[a]	–1.209[b]	0.141[b]	–0.001	0.175	–	17.086	0.389
	–0.187[a]	–1.267[b]	0.144[b]	–0.005	0.189	0.012	18.799	0.362
Deep GM	–0.016[c]	–	–	–	–	–	–29.356[c]	0.061[c]
	–0.018	0.034	–	–	–	–	–27.785	0.034
	–0.027	–0.065	0.012	–	–	–	–26.087	–0.001
	–0.029	–0.043	0.010	0.011	–	–	–24.800	–0.023
	–0.027	–0.035	0.009	0.010	–0.018	–	–22.922	–0.075
	–0.028	–0.086	0.011	0.007	–0.005	0.011	–22.194	–0.079

Note:—The en dash indicates that term was not included in model; aR^2, adjusted R^2.
[a] $P < .005$.
[b] $P < .05$.
[c] Model with lowest Akaike Information Criterion.

However, the HbA1c effect was reduced in the presence of DKA, suggesting that reductions in NAA/Cr due to DKA may outweigh those due to increased HbA1c.

DISCUSSION

MRSI Image Processing in Children with T1D

We found 2D MRSI to be an effective tool for identifying localized tissue-weighted NAA/Cr differences in children with T1D across multiple sites. On an individual level, we identified higher NAA/Cr in the WM than in deep GM, consistent with prior studies in healthy adults.[24] On the population level, we found negative associations with complications of T1D in WM, specifically reduced NAA/Cr with chronic hyperglycemia and DKA, as discussed in following sections.

In children with T1D, MRS has been used as single-voxel spectroscopy in single-site case reports.[13-16] Single-voxel spectroscopy has the benefit of allowing investigators to place a voxel in tissue as desired to measure metabolite ratios in a single location in the brain with higher signal-to-noise ratios.[25] However, this approach makes it difficult to resolve tissue or region differences in metabolite ratios across the brain with a single acquisition or to retroactively analyze other locations that were not prospectively defined.[25] We demonstrate that 2D MRSI, even with a lower signal-to-noise ratio than single-voxel spectroscopy, when combined with weighted signal averaging, overcomes these limitations in pediatric T1D samples at multiple sites. This suggests that future, large-scale, multisite MRS studies that are better equipped to sample diverse participants from this population can benefit from 2D imaging.

As it stands, there is no widely accepted methodology for identifying region-specific metabolite ratios from 2D MRSI, largely due to 3 key challenges. The first is accounting for partial volume effects among different brain tissues. The second is accounting for magnetic field inhomogeneities, eddy currents, and other nonlinearities that may exist across large structures or spatial dependencies like those due to chemical shift displacement. The third is accounting for noise that can exist in every single step of MRSI analysis, including signal acquisition, frequency transformation, spectral baseline modeling, basis fitting, and peak computation. Existing techniques using linear regression or

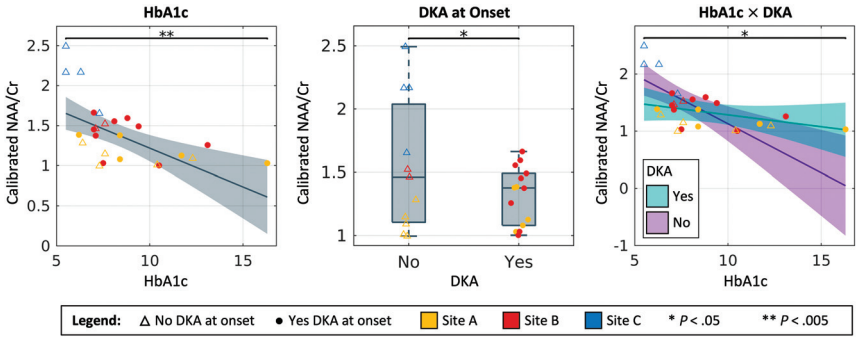

FIG 5. Associations of NAA/Cr in WM with T1D complications. The calibrated NAA/Cr ratios in WM are shown plotted against HbA1c, DKA status, and their interaction. Data points are colored by site with the symbol denoting the participant's DKA status.

source separation methods have primarily focused on overcoming partial volume effects.[24,26,27] However, we note that these techniques are performed later in the MRSI workflow and risk compounding and propagating noise, yielding measurements with reduced meaning. Thus, we propose first performing the weighted averaging operation in the signal domain without explicit partial volume modeling to exchange increased tissue specificity for reduced noise artifacts. Accordingly, we emphasize that the results reported here are "weighted" by tissue as opposed to being absolutely "specific" to tissue. We note that this design choice was made in large part due to considerations for noisy and variable data that may arise from multisite studies. Furthermore, we note that no approach has yet successfully modeled spatial inhomogeneities, dependencies, and nonlinearities. Thus, in the future, we hope for sequences with higher signal-to-noise ratios and to extend this idea of regional mapping in the signal domain with posterior matrix inversions to better incorporate partial volume effects and to add direct consideration of spatial nonlinearities, extending emerging methodologies.[24,26,27]

When computing metabolite ratios with LCModel, we leveraged "default" 3T basis sets provided by LCModel instead of computing "custom," scanner-specific sets using pulse sequences and envelope parameters.[28,29] This design choice was made for the following reasons: 1) to simplify both the present and future studies across multiple sites where MRSI pulse sequences and envelope parameters may not be readily available or reliably queried from scanners (as was the case for sites B and C presently); 2) because custom basis sets leveraging techniques like density operator simulation or the Versatile Simulation, Pulses, and Analysis (VeSPA; https://www.opensourceimaging.org/project/vespa-versatile-simulation-pulses-analysis/) toolkit primarily impact multiplet signals, whereas NAA and Cr are largely singlet;[28-30] and 3) because initial attempts using these custom sets did not dramatically affect results.

We used data from multiple sites acquired with different TE/TRs to maximize the sample size available for analysis. Thus, this approach required empiric calibration for site-wise effects via phantom studies for this pilot study. However, scanner calibration is an open problem, and many other calibration options exist. Careful consideration of site-wise effects should be used in future studies, including the use of matched TE/TR acquisitions and scanner hardware when possible.

WM NAA/Cr and Chronic Hyperglycemia

We found a negative association between WM NAA/Cr and hyperglycemia, as measured by HbA1c, that was not present in the deep GM. HbA1c is an average measure of chronic glucose control in the 3 months preceding the measurement.[31] Thus, we interpret this negative association as evidence that prolonged hyperglycemia is associated with neuroaxonal loss in WM diffusely in children with T1D. This finding builds on prior DTI studies in this population that have suggested a relationship between hyperglycemia and WM biomarkers and represents a novel exploration of diffuse WM neurochemistry, as opposed to focal investigations performed in prior single-voxel MRS studies.[8,13-16]

While small sample sizes can produce underpowered or overfit models, we are reassured that this effect was significant throughout the forward model selection process and was not suppressed by additional covariates. Furthermore, we found that the best model identified through model selection explained roughly 40% of the variance in the data, indicating high explainability in a noisy system with a small sample size. Thus, we hope these small-scale, exploratory results serve as evidence to motivate larger multisite studies to elaborate on these findings. Notably, larger-scale studies should further investigate the clinical implications of these findings and their associations with cognitive outcomes. Additionally, given that HbA1c is an average measurement of blood sugar across time, future studies could clarify which aspects of glycemic variability are most impactful, including time spent in the target glucose range, daily excursions, pre- and postprandial levels, and the number of hyper- or hypoglycemic episodes.[32] Inclusion of continuous glucose monitoring data may allow these effects to be characterized.

We note the absence of an age effect in our results. Prior MRS studies have established age effects in NAA and Cr at low TEs (around 30 ms) in children.[33] However, different TEs, such as the long TEs used presently (>100 ms), affect different peaks differently, and changing NAA and changing Cr do not equate to changing NAA/Cr, especially in a small sample. Thus, to balance the need for modeling age against the differences between metabolite- and ratio-based analyses as well as the uncertainties of MRS at different TEs, we included age as a variable during model selection as opposed to explicitly acquiring a control group for age in this pilot study.

WM NAA/Cr and DKA

We found throughout the model selection process that participants with DKA at disease onset had a decreased WM NAA/Cr, similar to the HbA1c effect, and that the HbA1c effect was muted in the presence of DKA. However, we found that these effects were only revealed when considered jointly with and in the context of HbA1c via inclusion of an interaction term between the two. DKA is a well-known complication of T1D, marked by an acute elevation of blood sugar to dangerous levels coupled with the onset of acidosis due to the development of ketones, potential cerebral edema, and other metabolic changes.[34] Thus, these associations suggest that WM neuroaxonal integrity may be diffusely affected by episodes of DKA in a manner that outweighs chronic changes from prolonged hyperglycemia.

As mentioned previously, the primary limitation to this interpretation is the potential confounding by site. Differences in DKA frequency by site as well as site effects that may be larger in magnitude than glycemic effects make it difficult to untangle the two. Another limitation is that patients with frequent episodes of DKA may also have higher HbA1c levels.[35] Moreover, due to the multifactorial nature of DKA, it is unclear which of its aspects may be contributing to these findings. Furthermore, we investigated the presence of DKA at the onset of T1D, but due to sample size limitations, we were not able to account for DKA severity or subsequent episodes.

In short, we recognize that neurophysiologic changes in T1D are multifactorial and did not account for all possible variables in this pilot study. We note that this limitation is common in other neuroimaging studies examining brain structure and function in T1D, including those with larger sample sizes.[36] One large-scale study in which the number of DKA episodes, severity of DKA, hyperglycemia, hypoglycemia, and duration of T1D were simultaneously accounted for only considered behavioral outcomes without neuroimaging.[37] Despite our small sample size, however, we found significant effects that were not suppressed, even as additional covariates were added. Thus, these small-scale associations support that larger studies of WM health in T1D should do the following: 1) consider interactions between acute T1D complications, like DKA, and chronic glucose control, and 2) take into account balanced DKA groups per site and rigorous harmonization of different acquisition and scanner effects, as mentioned previously.

Last, we note that both the DKA and HbA1c effects were seen only in the WM and not in GM. This finding is consistent with other studies that have found reductions in WM volume in children 6 months after DKA and reductions in WM structural integrity.[38-40] Thus, we would expect NAA/Cr to be reduced in WM related to neuroaxonal loss. Other studies have also found reductions in GM volume in individuals with T1D, and it has been posited that patients with long-standing T1D may have partial neuronal loss or dysfunction related to their disease.[41,42] Our findings may indicate that cerebral WM is more vulnerable to glycemic injury, and we suspect that a reduction in GM NAA/Cr would also be seen if our participants had long-standing T1D. Alternatively, the absence of effects in GM may simply be related to the small sample size in this pilot study.

CONCLUSIONS

Our pilot study represents a step toward understanding the neurophysiology underlying brain changes in T1D, elucidating its relationship to complications of T1D, and characterizing how MRSI and MR imaging may be integrated to monitor brain health. For instance, studies have shown alterations in cerebral WM structure and reduced WM volume in children with T1D using structural and diffusion tensor imaging and that these WM changes are associated with reduced neurocognitive scores.[43-45] Thus, there are clear clinical ramifications for this work, and using MRSI adds to our understanding of potential mechanisms of injury. Furthermore, neuroimaging is not currently part of the monitoring algorithm for individuals with T1D. However, assessment for subtle neurologic injury with MR imaging of the brain is recommended at least once in childhood and once in adulthood in a different chronic illness in which WM injury may lead to changes in clinical care.[46] One can thus envision how assessing neuroaxonal loss or dysfunction might be clinically relevant for T1D.

We present a novel exploration of tissue-weighted MRSI in children with T1D and a first attempt to untangle the effects of DKA and chronic hyperglycemia on neuronal integrity in different tissues across the brain in this population. We found that MRSI differentially identified NAA/Cr in T1D by tissue and complications of T1D were associated with markers of neuroaxonal loss in WM. Our study has 3 key limitations: 1) reduced tissue-specificity and spatial homogeneity in exchange for tissue-weighting with improved signal-to-noise, 2) reduced power due to limited sample sizes, and 3) large site effects. However, the notable public health implications for this population and our preliminary findings motivate the need for higher signal-to-noise 2D MRSI sequences and innovative analysis methods that explicitly consider partial volume effects and spatial nonlinearities. Moreover, these new methods should be leveraged in large-scale, harmonized multisite MRSI and MR imaging studies to better understand and monitor changes in brain neurochemistry and neurocognition in children with T1D.

Disclosure forms provided by the authors are available with the full text and PDF of this article at www.ajnr.org.

REFERENCES

1. Centers for Disease Control and Prevention. **National Diabetes Statistics Report: Estimates of Diabetes and Its Burden in the United States.** 2020. https://www.cdc.gov/diabetes/data/statistics-report/index.html. Accessed September 10, 2020
2. Cato A, Hershey T. **Cognition and type 1 diabetes in children and adolescents.** *Diabetes Spectr* 2016;29:197–202 CrossRef Medline
3. Jaser SS, Jordan LC. **Brain health in children with type 1 diabetes: risk and protective factors.** *Curr Diab Rep* 2021;21:12 CrossRef Medline
4. Mauras N, Mazaika P, Buckingham B, et al; Diabetes Research in Children Network (DirecNet). **Longitudinal assessment of neuroanatomical and cognitive differences in young children with type 1 diabetes: association with hyperglycemia.** *Diabetes* 2015;64:1770–79 CrossRef Medline
5. Mazaika PK, Weinzimer SA, Mauras N, et al; Diabetes Research in Children Network (DirecNet). **Variations in brain volume and growth in young children with type 1 diabetes.** *Diabetes* 2016;65:476–85 CrossRef Medline
6. Hershey T, Perantie DC, Wu J, et al. **Hippocampal volumes in youth with type 1 diabetes.** *Diabetes* 2010;59:236–41 CrossRef Medline
7. Foland-Ross LC, Reiss AL, Mazaika PK, et al; the Diabetes Research in Children Network (DirecNet). **Longitudinal assessment of hippocampus structure in children with type 1 diabetes.** *Pediatr Diabetes* 2018;19:1116–23 CrossRef Medline
8. Antenor-Dorsey JA, Shimony JS, Hershey T. **Diffusion tensor imaging of the brain in type 1 diabetes.** *Eur Med J Diabetes* 2014;2:42–47 CrossRef
9. Foland-Ross LC, Tong G, Mauras N, et al; Diabetes Research in Children Network (DirecNet). **Brain function differences in children with type 1 diabetes: a functional MRI study of working memory.** *Diabetes* 2020;69:1770–78 CrossRef Medline
10. Musen G, Simonson DC, Bolo NR, et al. **Regional brain activation during hypoglycemia in type 1 diabetes.** *J Clin Endocrinol Metab* 2008;93:1450–57 CrossRef Medline

11. Šuput Omladicõ J, Slana Ozimicõ A, Vovk A, et al. **Acute hyperglycemia and spatial working memory in adolescents with type 1 diabetes**. *Diabetes Care* 2020;43:1941–44 CrossRef Medline
12. Gallardo-Moreno GB, González-Garrido AA, Gudayol-Ferré E, et al. **Type 1 diabetes modifies brain activation in young patients while performing visuospatial working memory tasks**. *J Diabetes Res* 2015;2015:703512 CrossRef Medline
13. Wootton-Gorges SL, Buonocore MH, Kuppermann N, et al. **Cerebral proton magnetic resonance spectroscopy in children with diabetic ketoacidosis.** *AJNR Am J Neuroradiol* 2007;28:895–99 Medline
14. Wootton-Gorges SL, Buonocore MH, Caltagirone RA, et al. **Progressive decrease in N-acetylaspartate/creatine ratio in a teenager with type 1 diabetes and repeated episodes of ketoacidosis without clinically apparent cerebral edema: evidence for permanent brain injury.** *AJNR Am J Neuroradiol* 2010;31:780–81 CrossRef Medline
15. Sarac K, Akinci A, Alkan A, et al. **Brain metabolite changes on proton magnetic resonance spectroscopy in children with poorly controlled type 1 diabetes mellitus.** *Neuroradiology* 2005;47:562–65 CrossRef Medline
16. Ozturk A, Degaonkar M, Matson MA, et al. **Proton MR spectroscopy correlates of frontal lobe function in healthy children.** *AJNR Am J Neuroradiol* 2009;30:1308–14 CrossRef Medline
17. Mangia S, Kumar AF, Moheet AA, et al. **Neurochemical profile of patients with type 1 diabetes measured by 1H-MRS at 4 T.** *J Cereb Blood Flow Metab* 2013;33:754–59 CrossRef Medline
18. Huo Y, Xu Z, Xiong Y, et al. **3D whole brain segmentation using spatially localized atlas network tiles.** *Neuroimage* 2019;194:105–19 CrossRef Medline
19. Walfish S. **A review of statistical outlier methods.** *Pharmaceutical Technology* 2006;30:82–86
20. Provencher SW. **Estimation of metabolite concentrations from localized in vivo proton NMR spectra.** *Magn Reson Med* 1993;30:672–79 CrossRef Medline
21. Cai LY, Tanase C, Anderson AW, et al. **Multimodal neuroimaging in pediatric type 1 diabetes: a pilot multisite feasibility study of acquisition quality, motion, and variability.** In: Išgum I, Colliot O, eds. *Medical Imaging 2022: Image Processing*. Vol 12032. SPIE; 2022:135 CrossRef
22. Povazõan M, Mikkelsen M, Berrington A, et al. **Comparison of multivendor single-voxel MR spectroscopy data acquired in healthy brain at 26 sites**. *Radiology* 2020;295:171–80 CrossRef Medline
23. Graf C, MacMillan EL, Fu E, et al. **Intra- and inter-site reproducibility of human brain single-voxel proton MRS at 3 T.** *NMR Biomed* 2019;32:1–10 CrossRef Medline
24. Tal A, Kirov II, Grossman RI, et al. **The role of gray and white matter segmentation in quantitative proton MR spectroscopic imaging.** *NMR Biomed* 2012;25:1392–400 CrossRef Medline
25. Maudsley AA, Andronesi OC, Barker PB, et al. **Advanced magnetic resonance spectroscopic neuroimaging: experts' consensus recommendations**. *NMR Biomed* 2021;34:e4309 CrossRef Medline
26. Goryawala MZ, Sheriff S, Stoyanova R, et al. **Spectral decomposition for resolving partial volume effects in MRS.** *Magn Reson Med* 2018;79:2886–95 CrossRef Medline
27. Hetherington HP, Pan JW, Mason GF, et al. **Quantitative 1H spectroscopic imaging of human brain at 4.1 T using image segmentation.** *Magn Reson Med* 1996;36:21–29 CrossRef Medline
28. Lally PJ, Montaldo P, Oliveira V, et al; MARBLE Consortium. **Magnetic resonance spectroscopy assessment of brain injury after moderate hypothermia in neonatal encephalopathy: a prospective multicentre cohort study.** *Lancet Neurol* 2019;18:35–45 CrossRef Medline
29. Choi C, Ganji SK, DeBerardinis RJ, et al. **2-Hydroxyglutarate detection by magnetic resonance spectroscopy in IDH-mutated patients with gliomas.** *Nat Med* 2012;18:624–29 CrossRef Medline
30. Soher BJ, Semanchuk P, Todd D, et al. **VeSPA: Integrated applications for RF pulse design, spectral simulation and MRS data analysis.** *Mag Reson Med* 2023 May 15. [Epub ahead of print] CrossRef Medline
31. American Diabetes Association. **Glycemic targets: standards of medical care in diabetes—2021**. *Diabetes Care* 2021;44(Suppl 1):S73–84 CrossRef Medline
32. Lundholm MD, Emanuele MA, Ashraf A, et al. **Applications and pitfalls of hemoglobin A1C and alternative methods of glycemic monitoring.** *J Diabetes Complications* 2020;34:107585 CrossRef Medline
33. Holmes MJ, Robertson FC, Little F, et al. **Longitudinal increases of brain metabolite levels in 5-10 year old children.** *PLoS One* 2017;12:e0180973 CrossRef Medline
34. American Diabetes Association. **Diabetes care in the hospital: standards of medical care in diabetes-2021.** *Diabetes Care* 2021;44(Suppl 1):S211–20 CrossRef Medline
35. Ryan CM, van Duinkerken E, Rosano C. **Neurocognitive consequences of diabetes.** *Am Psychol* 2016;71:563–76 CrossRef Medline
36. Aye T, Mazaika PK, Mauras N, et al; Diabetes Research in Children Network (DirecNet) Study Group. **Impact of early diabetic ketoacidosis on the developing brain.** *Diabetes Care* 2019;42:443–49 CrossRef Medline
37. Ghetti S, Kuppermann N, Rewers A, et al; Pediatric Emergency Care Applied Research Network (PECARN) DKA FLUID Study Group. **Cognitive function following diabetic ketoacidosis in children with new-onset or previously diagnosed type 1 diabetes.** *Diabetes Care* 2020;43:2768–75 CrossRef Medline
38. Cameron FJ, Scratch SE, Nadebaum C, et al; DKA Brain Injury Study Group. **Neurological consequences of diabetic ketoacidosis at initial presentation of type 1 diabetes in a prospective cohort study of children.** *Diabetes Care* 2014;37:1554–62 CrossRef Medline
39. Antenor-Dorsey JA, Meyer E, Rutlin J, et al. **White matter microstructural integrity in youth with type 1 diabetes.** *Diabetes* 2013;62:581–89 CrossRef Medline
40. Fox LA, Hershey T, Mauras N, et al; Diabetes Research in Children Network (DirecNet). **Persistence of abnormalities in white matter in children with type 1 diabetes.** *Diabetologia* 2018;61:1538–47 CrossRef Medline
41. Seaquist ER. **The impact of diabetes on cerebral structure and function.** *Psychosom Med* 2015;77:616–21 CrossRef Medline
42. Stantonyonge N, Sampedro F, Méndez J, et al. **Structural gray and white matter differences in patients with type 1 diabetes and impaired awareness of hypoglycemia**. *J Clin Endocrinol Metab* 2021;106:450–58 CrossRef Medline
43. Aye T, Barnea-Goraly N, Ambler C, et al. **White matter structural differences in young children with type 1 diabetes: a diffusion tensor imaging study.** *Diabetes Care* 2012;35:2167–73 CrossRef Medline
44. Mauras N, Buckingham B, White NH, et al; Diabetes Research in Children Network (DirecNet). **Impact of type 1 diabetes in the developing brain in children: a longitudinal study.** *Diabetes Care* 2021;44:983–92 CrossRef Medline
45. Toprak H, Yetis H, Alkan A, et al. **Relationships of DTI findings with neurocognitive dysfunction in children with type 1 diabetes mellitus.** *Br J Radiol* 2016;89:20150680–15 CrossRef Medline
46. DeBaun MR, Jordan LC, King AA, et al. **American Society of Hematology 2020 guidelines for sickle cell disease: prevention, diagnosis, and treatment of cerebrovascular disease in children and adults.** *Blood Adv* 2020;4:1554–88 CrossRef Medline